Chapter II. **Structure and mechanical properties of genetically engineered protein hydrogels assembled through aggregation of leucine zipper peptide domains**

Abstract

The plateau storage modulus G'_∞ of an artificial protein hydrogel, which was constructed from a triblock protein (designated $AC_{10}A$) that contained two associative leucine-zipper endblocks and a water-soluble random coil midblock, was systematically studied under various pH values, concentrations, and ionic strengths. The normalized plateau storage modulus G'_∞/nkT is below 13% at all concentrations and pH values examined, suggesting that $AC_{10}A$ chains tend to form a substantial fraction of looped configurations according to Annable's model that relates network topology to modulus[1]. This was supported by a fluorescence quenching experiment: substantial quenching occurred in labeled d-$AC_{10}A$-a (d=tryptophan at the N-terminus, a=coumarin at the C terminus) chains mixed with a great excess of unlabelled $AC_{10}A$ chains. The tendency to form loops originates from the compact size of the random coil midblock (mean $R_{H(C10)}$~20 Å, determined from quasi-elastic light scattering of C_{10}). Despite the small aggregation number of the leucine zipper domains (tetrameric aggregates, determined from multi-angle static light scattering of AC_{10} diblock), the average center-to-center distance between aggregates in 7% w/v networks is roughly 3 times the radius of gyration ($R_g \approx 1.2$-$1.5\ R_H$) and 1.5 times the average end-to-end distance ($\sqrt{\langle R^2 \rangle} \approx 2.9$-$3.7\ R_H$) of the C_{10} domain. To avoid the energy penalty for stretching the C_{10} domain, the chains tend to form loops. The importance of loops explains the nonmonotonic effect of pH on

G'_∞ and the decrease in G'_∞ with increasing ionic strength. It also led to the design concept of increasing the mid-block length or charge density to increase G'_∞.

1. Introduction

Hydrogels have attracted both academic and practical interest over many years. Recently, hydrogels designed for application in biomedical engineering such as controlled release[2,3], cell immobilization[4], and tissue engineering[5] have drawn particular attention. Compared to hydrogels for traditional industrial applications, those to be used in biomedical fields must meet more stringent requirements. Besides physical properties, biological properties, such as nontoxicity and ability to incorporate appropriate biological determinants (e.g. cell-binding domains, enzyme recognition sites), are also essential[5-8]. The ability to systematically control structure and properties is especially important, which allows the materials to be optimized for clinical applications and systematically tuned to address fundamental biological questions.

Hydrogels currently used in research and clinical trials are formed from either natural biopolymers or chemically synthesized polymers[5]. Natural biopolymers often have biological functionality and are nontoxic, but sources are limited, properties are variable, opportunities for systematic control of structure and properties are limited, and concerns about viral contamination restrict the use of animal products in biomedical applications. On the other hand, chemically synthesized polymers address these shortcomings at the expense of biological functionality. Toxic residual monomers can compromise their safety.

Genetic engineering provides an opportunity to create biomaterials combining the advantages of both classes. Our group previously reported that a genetically engineered multidomain protein ($AC_{10}A$) consisting of two associative leucine zipper endblocks (A) and a random coil midblock (C_{10}) could assemble into hydrogels in aqueous solutions[9]. Leucine zippers are widely distributed in nature where they perform vital functions ranging from muscle contraction[10] to transcriptional regulation[11]. These domains are characterized by heptad repeating units designated *abcdefg*, where the *a* and *d* positions are occupied by hydrophobic residues such as leucine, and the *e* and *g* positions are occupied by charged residues. Each coiled-coil domain folds into an amphiphilic α-helix that places the *a* and *d* residues on a hydrophobic face. Hydrophobic interactions drive these helices to associate into oligomeric bundles. The properties of $AC_{10}A$ hydrogels, such as their viscosity, change with external stimuli including pH and temperature. This environmental responsiveness makes them intriguing for biomedical applications.

These hydrogels demonstrate an approach to creating a new category of biomaterials that have potential for many applications. Control of the physical properties of these hydrogels is essential for their biomedical applications. For example, it has been shown that rigidity of scaffold materials acts as an extracellular signal and plays a critical role in regulating cell adhesion, spreading, migration, and even survival[12-15]. However, understanding of the structure-property relationships of artificial protein hydrogels is limited. Important physical properties, such as their rigidity (storage modulus), have not been systematically characterized.

This chapter focuses on the structural properties that regulate storage moduli of $AC_{10}A$ hydrogels and provides molecular design principles to increase modulus. Storage

moduli of $AC_{10}A$ hydrogels were systematically characterized under various conditions of pH, concentration, and ionic strength using oscillatory shear measurements. Their structural properties were probed on microscopic and molecular levels using various techniques such as fluorescence resonance energy transfer and light scattering. On the basis of the structure-property relationships revealed from these investigations, two new materials exhibiting greater storage modulus were designed, synthesized and characterized.

2. Experimental section

2.1. Construction of expression vectors encoding artificial proteins

Amino acid sequences of the proteins to be discussed in this chapter are shown in Scheme 1. Expression vectors pQE9AC_{10}Acys, pQE9AC_{10}Atrp, pQE9Acys, pQE9Atrp, and pQE9C_{10}trp were constructed previously by Petka[16]. The expression vector pQE9cysA was constructed previously by Gallivan.

To construct pQE9C_{10}Acys, a DNA segment encoding C_{10} was excised from pQE9C_{10}trp by digestion with *Nhe*I and *Spe*I (New England Biolabs, Beverly, MA), and ligated into the pUC18L2A[16] plasmid at the *Nhe*I site. A DNA fragment encoding C_{10}Acys was excised from the resulting plasmid pUC18L2C_{10}A by digestion with *Bam*HI, and ligated into the *Bam*HI site of the pQE9 expression vector to yield pQE9C_{10}Acys.

A DNA segment encoding C_{10}A was excised from pUC18L2C_{10}A by digestion with *Nhe*I and *Spe*I, and ligated into the *Spe*I site of the plasmid pQE9A-no-trp (constructed previously by Tang[17]) to yield the plasmid pQE9AC_{10}A-no-trp.

DNA segments encoding AC_{10}, $AC_{26}A$, and $A[AGPEG]_{18}A$ were excised from $pUC18L2AC_{10}$, $pUC18L2AC_{26}A$ (constructed previously by Petka[16]), and $pUC18L2A[AGPEG]_{18}A$ (constructed previously by Murata), respectively, by digestion with *Nhe*I and *Spe*I, and each was ligated into the pUC18L1[16] cloning vector digested at the *Nhe*I and *Spe*I sites. DNA fragments encoding AC_{10}trp, AC_{26}Atrp and $A[AGPEG]_{18}$Atrp were excised from the resulting $pUC18L1AC_{10}$, $pUC18L1AC_{26}A$, and $pUC18L1A[AGPEG]_{18}A$, respectively, by digestion with *Bam*HI, and each was ligated into the *Bam*HI site of the pQE9 vector to yield $pQE9AC_{10}$trp, $pQE9AC_{26}$Atrp, and $pQE9A[AGPEG]_{18}$Atrp.

The sequences of all newly constructed expression vectors were verified at the DNA sequencing core facility of the Beckman Institute at the California Institute of Technology.

2.2. Protein synthesis and purification

Expression vectors were each transformed into *Escherichia coli* strain SG13009, which carries the repressor plasmid pREP4 (Qiagen, Chatsworth, CA). Cultures of these cells were each grown at 37 °C in 1 L of Terrific Broth (TB) supplemented with 200 mg/L of ampicillin (Sigma, St. Louis, MO) and 50 mg/L of kanamycin (Sigma, St. Louis, MO). The culture was induced with 1.5 mM isopropyl-1-β-D-thiogalactoside (IPTG) (Calbiochem, Inc., San Diego, CA) when it reached an optical density (600 nm) of 0.7~1. Protein expression continued for 5 hours; the optical density reached 1.4~2. Cells were harvested by centrifugation (5 min, 10,000 g); typical yields were ca. 5 g of wet cell mass per liter of cell culture. The cell pellet was re-suspended in 8 M urea (pH 8.0) and frozen

at –80 °C. The thawed lysate was centrifuged at 22,100 g and 4 °C for 20 minutes and the supernatant was collected for purification. A 6×histidine tag encoded in the pQE9 vectors allows proteins to be purified by affinity chromatography on a nickel nitrilotriacetic acid resin (Qiagen, Chatsworth, CA) following the denaturing protocol provided by Qiagen. To prevent non-specific disulfide bond formation during purification for the proteins containing cysteine residues, 14 mM β–mercaptoethanol (Sigma, St. Louis, MO) was added to the washing and elution buffers. The eluted fractions were dialyzed against sterile deionized water for three days at room temperature and the proteins were lyophilized. The typical protein yield was 60-100 mg per liter of cell culture.

2.3. Chemical cleavage of the histidine tag from C_{10}trp and titration of the histidine-tag-free C_{10}trp solution

Cyanogen bromide (CNBr) was used to cleave the N-terminal histidine tag fused to C_{10}trp. The cleavage occurs at the C-terminal side of each methionine residue that flanks the C_{10} domain in C_{10}trp. C_{10}trp was dissolved in 6 M guanidine·HCl/0.2 M HCl at a concentration of 1 mg/mL. CNBr was added into the solution in a weight ratio (CNBr to C_{10}trp) of 50:1. The solution was sealed, purged with argon for half an hour, and stirred by a magnetic stirring bar for 24 hours at room temperature. Unreacted CNBr was removed with rotor vacuum at room temperature. Matrix-assisted laser desorption ionization mass spectrometry (MALDI-MS) conducted with a 10 mg/mL sinapinic acid matrix solution on a Voyager mass spectrometer (Applied Biosystems) revealed a single peak of mass 7081 Da. The mass shift from the intact protein (10383 Da) is 3302 Da, consistent with the sum of the expected masses of the cleaved segments

MRGSHHHHHHGSDDDDKASYRDP and PTSW. The histidine-tag-free C_{10}trp was dissolved in distilled deionized water at a concentration of 1325 μM. A 0.5 N NaOH solution (Mallinckrodt Baker, Inc., Phillipsburg, NJ) was diluted to different concentrations in the range between 1.5 mM to 30 mM, and each NaOH solution was mixed with the C_{10}trp solution in a volumetric ratio of 1:1. The pH value of each mixture was measured with a Corning ion analyzer 250.

2.4. Labeling Acys and AC_{10}Acys with coumarin

Coumarin was site-specifically ligated to the cysteine residues engineered at the C-termini of Acys and AC_{10}Acys, respectively. Protein solutions (100 μM) were each prepared in PBS buffer (10 mM NaH_2PO_4, 90 mM NaCl). A tris(2-carboxyethyl)phosphine hydrochloride (TCEP) (Pierce, Rockford, IL) stock solution (100 mM) was added into each protein solution to a final concentration of 2 mM. The pH of the mixture was adjusted to 4.5, followed by incubation at room temperature for half an hour to allow reduction of disulfide bonds. Then the pH was adjusted to 6.5. A 7-diethylamino-3-(4'-maleimidylphenyl)-4-methylcoumarin (CPM, Molecular Probes, Eugene, OR) stock solution (100 mM) was freshly prepared in DMSO, and added into each reduced protein solution to a concentration of 1 mM. The mixture was incubated in the dark at room temperature for half an hour. Additional labeling reagent (10 moles of 7-diethylamino-3-(4'-maleimidylphenyl)-4-methylcoumarin for each mole of protein) was added, and the mixture was incubated for an extra half hour. The sample was concentrated from 10 mL to 1 mL with Centricon YM-3 centrifugal filter unit (molecular weight cutoff 3000, Millipore, Billerica, MA), followed by gel filtration on a Sephadex

G-25 (Amersham Biosciences, Piscataway, NJ) column (1.5 cm diameter × 30 cm height) to remove unreacted dye. The protein fraction was collected, dialyzed against sterile deionized water, and lyophilized in the dark.

The signal corresponding to unmodified Acys in the MALDI mass spectrum (with a 10 mg/mL sinapinic acid matrix solution) almost disappeared. The area of the unreacted AC_{10}Acys peak in the mass spectrum was ca. 10% of the total peak area. However, the absorbance at 393 nm on a Cary 50 Bio UV-vis spectrophotometer (Varian, Palo Alto, CA) showed ca. 83% of Acys and ca. 70% of AC_{10}Acys was labeled, respectively, using the extinction coefficient of 28000 M^{-1} cm^{-1} for CPM[18].

2.5. Rheological measurements

Protein solutions were prepared in phosphate buffer (13 mM $NaH_2PO_4 \cdot H_2O$, 87 mM $Na_2HPO_4 \cdot 7H_2O$) with the pH value adjusted as needed. Each solution was centrifuged to remove entrapped bubbles and then loaded on an RFS III rheometer (TA Instruments, New Castle, Delaware). The temperature was controlled at 22.0 ± 0.1 °C by a Peltier thermoelectric device. A cone-and-plate geometry (0.04 rad cone angle and 25 mm diameter) was used to acquire dynamic mechanical spectra from 100 rad/s to 0.001 rad/s. To reduce the sample size, a parallel-plate geometry (0.5 mm gap and 8 mm diameter) was used for frequency sweep measurements from 100 rad/s to 1 rad/s to determine the plateau storage modulus. The plateau storage modulus for a given sample determined in these two different geometries differed by less than 7.5%. The edge of each sample was covered with mineral oil to minimize solvent evaporation. All frequency

sweep measurements were performed at a 1% strain, which was confirmed to be within the linear viscoelastic regime from strain sweep tests.

2.6. Fluorescence measurements

Solutions of Acys (W-A) and coumarin modified Acys (W-A-CPM) were each prepared in 100 mM phosphate buffer (pH 7.6) at a concentration of 100 μM. The solutions were subjected to fluorescence measurements on a fluorometer (Photon Technology International, Inc., Lawrenceville, NJ) at an excitation wavelength of 300 nm. Emission scans from 308 nm to 590 nm were recorded.

A solution of AC_{10}A-no-trp was prepared in 100 mM phosphate buffer (pH 7.6) at a concentration of 1.25%. Stock solutions of AC_{10}Acys (W-AC_{10}A) and coumarin modified AC_{10}Acys (W-AC_{10}A-CPM) were added into the AC_{10}A-no-trp solution, respectively, in a molar ratio of 1:25. The total protein concentration was 1.05% after the mixing. The AC_{10}A-no-trp solution, the mixture of AC_{10}A-no-trp and W-AC_{10}A, and the mixture of AC_{10}A-no-trp and W-AC_{10}A-CPM were subjected to fluorescence measurements on a fluorometer (Photon Technology International, Inc., Lawrenceville, NJ) at an excitation wavelength of 300 nm. Emission scans from 308 nm to 590 nm were recorded.

2.7. Quasi-elastic light scattering

Quasi-elastic light scattering measurements for a pH 10.0, 140 μM C_{10}trp solution were performed with BI-9000AT (Brookhaven, NY) and WyattQELS (Wyatt Technology Corporation, CA) digital autocorrelators. Since it was known that dimensions of C_{10} chains are smaller than 0.02 μM on the basis of release measurements for the 0.02 μM

fluorescent beads entrapped in AC_{10}Acys(L11c) gels (discussed in Chapter V), samples were filtered through 0.02 μM filters prior to measurements on the Brookhaven instrument. This step was not performed prior to measurements on the Wyatt instrument. The correlation function was analyzed with software (based on the CONTIN algorithm) provided by Brookhaven.

2.8. Multi-angle static light scattering

Solutions of AC_{10}trp were prepared in 100 mM phosphate buffer (pH 7.6) at concentrations of 0.179 mg/mL, 0.362 mg/mL, 0.540 mg/mL, and 0.721 mg/mL by weighing at least 3 mg of the protein on a microbalance with an error less than 0.05 mg. The solutions were each filtered through a 0.2 μM filter and subjected to multi-angle light scattering measurements on a DAWN EOS light scattering instrument (Wyatt Technology Corporation, CA). The data were analyzed using the Zimm formalism and a dn/dc value of 0.185[19].

2.9. Determination of strand orientation in leucine zipper aggregates using electrophoresis

Solutions of cysA and C_{10}Acys were prepared in 100 mM phosphate buffer at a concentration of 400 μM and mixed in a volumetric ratio of 1:1. The pH of the mixture was adjusted to 8.0, followed by incubation at room temperature under air for 48 hrs. A redox buffer (125 μM reduced glutathione, 62.5 μM oxidized glutathione, 1M NaCl, 50 mM MOPS, pH 7.5)[20] was then added into the mixture in a volumetric ratio of 1:1, followed by incubation at room temperature for 3 hrs. Electrophoresis of the solutions

was performed on 12% PAGE using the standard protocol with dithiothreitol omitted from the sample buffer. The gel was stained with Coomassie Brilliant Blue R-250. The relative intensity of protein bands was analyzed using NIH ImageJ (http://rsb.info.nih.gov/ij/).

3. Results

3.1. Plateau storage moduli of artifical protein hydrogels

The linear viscoelastic region for $AC_{10}A$ hydrogels extends up to a 10% strain according to strain sweep tests. Within the linear region, these hydrogels exhibit typical viscoelastic behavior (Figure 2.1): on short time scales (high frequencies), the storage modulus G' is nearly constant ($\approx G'_{\infty}$, plateau storage modulus) and is much greater than the loss modulus G''; on time scales longer than a characteristic relaxation time (τ_r) associated with the dominant loss peak, they behave more like viscous liquids ($G'' > G'$) and approach terminal behavior ($G' \sim \omega^2$ and $G'' \sim \omega$)[21] (Figure 2.1). The transition is also indicated by a crossover in G' and G'' at $\omega_x \sim 1/\tau_r$.

G'_{∞} of $AC_{10}A$ hydrogels increases nonlinearly with concentration (Figure 2.2). The normalized plateau storage modulus G'_{∞}/nkT (nkT is the modulus of an ideal network of n chains per unit volume in which 100% chains are elastically effective) increases with concentration, suggesting variation in network structure. Note that even at a concentration of 9% w/v, the value of G'_{∞}/nkT is only ca. 13%, significantly less than is observed in hydrogels formed from many other telechelic polymers, such as hydrophobic end-capped poly(ethylene glycol)s[1].

G'_∞ varies nonmonotonically with pH between 7 and 10 (Figure 2.3). For 7% w/v $AC_{10}A$ hydrogels, G'_∞ increases with pH between 7 and 8, then levels off, and starts to drop when pH is above 9.0. Over the whole pH range examined, G'_∞/nkT is less than 7%.

G'_∞ of $AC_{10}A$ hydrogels decreases with increasing buffer and salt concentrations (Figure 2.4).

When the midblock C_{10} (90 amino acids) was replaced by C_{26} (234 amino acids), G'_∞ of the resulting hydrogel increases 1.7 fold at the same weight concentration (7% w/v), and G'_∞/nkT increases 2.4 fold (Figure 2.5 and Figure 2.6). Increasing the charge density on the midblock while keeping its contour length fixed also increases G'_∞: when the midblock C_{10} (containing 10 charged residues when fully deprotonated) is replaced by $[AGPEG]_{18}$ (containing 18 charged residues when fully deprotonated), G'_∞ doubles (Figure 2.5, Figure 2.6).

3.2. Fluorescence resonance energy transfer

Fluorescence resonance energy transfer (FRET) was used to examine whether any leucine zipper strands orient antiparallel in tetrameric aggregates. The tryptophan-coumarin pair, which has a Föster distance of 31 Å[22] and has been used to probe structure and interactions of biopolymers[23,24], was selected as the donor-acceptor pair. Tryptophan was genetically engineered at the N-terminus of the isolated A domain, and coumarin was site-specifically ligated to the C-terminal cysteine. Site-specific labeling was suggested by the absence of peaks corresponding to multiple-site labeling. Mass spectral analysis revealed a mass shift of 393 Da after labeling (the molecular weight of 7-diethylamino-3-(4'-maleimidylphenyl)-4-methylcoumarin is 402.25). The peak corresponding to

unlabeled protein almost disappeared in the mass spectrum, but the extent of labeling determined by UV-vis absorbance is about 83% on the basis of an extinction coefficient of 28000 $M^{-1}cm^{-1}$ at 393 nm for CPM[18].

In the presence of C-terminal coumarin, the tryptophan fluorescence between 308 and 410 nm was strongly quenched (Figure 2.7). The quenching efficiency is estimated to be ca. 85-90% on the basis of $E=1-(F_{DA}/F_D)$, where F_{DA} and F_D are the donor fluorescence in the presence and absence of the acceptor, respectively (fluorescence intensities are based on the areas of the peaks between 308 and 410 nm). No obvious concentration dependence of the quenching efficiency was observed (Figure 2.8), suggesting that the quenching of the donor fluorescence does not result from random collision of different aggregates. Since the Föster distance for the tryptophan-coumarin pair is 31 Å and the leucine zipper is 65 Å in length[25], the energy transfer from a tryptophan to the coumarin on the same strand is negligible. This leads to the conclusion that the strong energy transfer occurs within each aggregate when the N-terminal tryptophan and the C-terminal coumarin are brought into proximity by antiparallel strands.

The FRET technique was also used to probe intramolecular loops in an $AC_{10}A$ solution. When $AC_{10}A$ chains labeled with a donor fluorophore at one end and an acceptor fluorophore at the other (W-$AC_{10}A$-CPM) were mixed with a great excess of unlabeled $AC_{10}A$ ($AC_{10}A$-no-trp) chains in a solution, FRET occurs only when labeled chains adopt looped configurations. Tryptophan was genetically engineered at the N-terminus of $AC_{10}A$cys, and coumarin was site-specifically ligated to the C-terminal cysteine. The area of the peak corresponding to unlabeled protein in the mass spectrum

was about 10% of the total area. But the extent of labeling determined by UV-vis absorbance was about 70% on the basis of an extinction coefficient of 28000 $M^{-1}cm^{-1}$ at 393 nm for CPM[18].

A 1.25% w/v $AC_{10}A$-no-tr solution showed negligible fluorescence emission peak between 308 and 410 nm at an excitation wavelength of 300 nm (Figure 2.9). When $AC_{10}Acys$ (W-$AC_{10}A$) was added in the $AC_{10}A$-no-trp solution in a molar ratio of 1:25 (the total protein concentration changed slightly to 1.05% after mixing), a pronounced fluorescence emission peak between 308 and 410 nm was observed. When coumarin modified $AC_{10}Acys$ (W-$AC_{10}A$-CPM) was similarly added in the $AC_{10}A$-no-trp solution, the fluorescence emission between 308 and 410 nm was reduced compared to that in the absence of coumarin (Figure 2.9). At the same time a significant fluorescence peak between 410 and 590 nm was observed. Given the extent of labeling is about 70%, the average quenching efficiency (E) for labeled chains is estimated to be ca. 75% on the basis of $E=[1-(F_{DA}/F_D)]/f$, where F_{DA} is the donor fluorescence with acceptor present, F_D is the donor fluorescence without acceptor present, and f is the extent of labeling (fluorescence intensities are based on the areas of the peaks between 308 and 410 nm). Significant quenching of tryptophan fluorescence suggests that loops form readily in $AC_{10}A$ solutions. Measurements at higher protein concentrations failed, because the fluorescence of the tyrosine residue in $AC_{10}A$-no-trp was not negligible and the solution does not provide a good nonfluorescent background at a concentration as high as 5% w/v. In any case, the measurement at the low concentration qualitatively proved a strong tendency of $AC_{10}A$ chains to adopt looped configurations.

3.3. Light scattering

Multi-angle static light scattering measurements for solutions of a diblock protein AC_{10}trp revealed the aggregation number of the associative leucine zipper domain. Light scattering signals from AC_{10}trp solutions at concentrations of 11 μM, 22 μM, 33 μM and 44 μM were analyzed using a Zimm plot (Figure 2.10). The analysis revealed that the molar mass of the dominant species is 64740 Da, close to the expected molar mass for tetramers (65336 Da). The scattering signals from a 123 μM AC_{10}trp solution were analyzed using a Debye plot with an input second virial coefficient of -6.5×10^{-4} mol mL/g^2 (revealed from the Zimm plot discussed above), giving a molar mass of 64400 Da. Tetrameric association of the leucine zipper domain suggested by multi-angle light scattering measurements agrees with analytical ultracentrifugation and small angle x-ray scattering studies conducted by Kennedy[26] previously. Analytical ultracentrifugation studies on solutions (less than 1 mM) of the isolated leucine zipper A suggest that it forms tetrameric bundles. But the effect of the attached midblock was not revealed from these experiments. Data from small angle x-ray scattering studies performed on AC_{10}A solutions at concentrations as high as 7% w/v (ca. 6.3 mM leucine zipper) fit well to a cylindrical model for tetrameric helical bundles with the following dimensions: length 63 Å, radius 13.6 Å, and a 1 Å axial pore. Thus, for the leucine zipper A, tetrameric association was found for the A domain alone, AC_{10} diblocks and AC_{10}A hydrogels; tetrameric association persisted over concentrations ranging from 11 μM to 6 mM.

Quasi-elastic light scattering measurements for C_{10}trp solutions (pH 10.0) were performed on a BI-9000AT and a WyattQELS digital autocorrelator, respectively. The

latter had superior dynamic capacity at the short time range relevant to C_{10}. Since it was known that dimensions of C_{10} chains are smaller than 0.02 μM on the basis of release measurements for the 0.02 μM fluorescent beads entrapped in AC_{10}Acys(L11c) gels (discussed in Chapter V), samples were filtered through 0.02 μM filters prior to measurements on the Brookhaven instrument. This step was not performed prior to measurements on the Wyatt instrument, so that a small tail above 60 μs was observed due to impurity particles. The signals in the tail were ignored. The two sets of measurements are in good accord at correlation times from 10 to 60 μs; together the measurements span from 1 to 10^4 μs (Figure 2.11). The time correlation function was analyzed with software on the basis of the CONTIN algorithm, revealing a mean hydrodynamic radius (R_H) of 20 Å. Since the ratio of radius of gyration to hydrodynamic radius (R_g/R_H) for polymer chains in solutions above the θ temperature is ca. 1.2~1.5[27,28], and the ratio of root-mean-square end-to-end distance to radius of gyration ($\sqrt{\langle R^2 \rangle}/R_g$) is ca. $\sqrt{6}$ [29-31], the radius of gyration and the average end-to-end distance of the C_{10} domain is ca. 24~30 Å and 59~73 Å, respectively.

These experimentally revealed dimensions are slightly larger than the dimensions under θ conditions predicted on the basis of scaling laws for denatured polypeptides and proteins[32-35]. Under θ conditions, the characteristic ratio $\langle R^2 \rangle / n_p l_p^2$ ($\langle R^2 \rangle$ is mean square end-to-end distance, n_p is the number of peptide bonds, l_p is the distance between adjacent α-carbon atoms (ca. 3.8 Å)) for denatured proteins that have the naturally occurring average distribution of amino acid residues is larger than 4[33-35]; however, it is greatly reduced when the fraction of glycine residues becomes significant[32]. Sequential

copolypeptides containing glycine, proline, and alanine have a characteristic ratio of 2.0~3.2 when the mole fraction of glycine is above 50%[32]. Since the mole fraction of glycine in the C_{10} domain is close to 50% and circular dichroism analysis suggests that it does not have secondary structure[16], its average end-to-end distance is estimated to be 51~64 Å under θ conditions.

3.4. Titration of the histidine-tag-free C_{10}trp solution

Although the pKa value of an isolated glutamic acid residue is 4.4, titration of a midblock (C_{10}) solution revealed a buffering regime between pH 7 and 8 (Figure 2.12), suggesting that deprotonation of the glutamic acid residues in the midblock extended into this pH regime. This change in pKa lies within the range of pKa shifts induced by hydrophobic residues[36] and charged residues in proximity.

3.5. Determination of strand orientation in leucine zipper aggregates using electrophoresis

The orientation of leucine zipper strands in aggregates was also examined with electrophoresis of mixtures of cysA and C_{10}Acys solutions. These two proteins have different molar masses (8394 Da and 16595 Da, respectively) and bear cysteine residues at the N-terminus and C-terminus, respectively. Solutions of cysA and C_{10}Acys were mixed and incubated at pH 8.0 for 48 hrs to allow strand exchange. If antiparallel orientation exists, the cysteines at the N-terminus of cysA and the cysteines at the C-terminus of C_{10}Acys would be brought into proximity, and some of them would be linked through thiol-disulfide exchange when a redox buffer was added. The linked

heterodimers have a different molar mass (24989 Da) from those of the species in unmixed solutions and could be resolved using electrophoresis.

When solutions of cysA and C_{10}Acys were mixed, incubated (pH 8.0, 48 hrs), and then exposed to redox buffer (3 hrs), linked heterodimers were observed (Figure 2.13). A band located between the dimer C_{10}Acys (molar mass 33190 Da) and the monomer C_{10}Acys (molar mass 16594 Da) was observed in mixture solutions, but not observed in unmixed solutions, suggesting existence of antiparallel leucine zipper strands in their aggregates. Relative protein concentration analyzed using NIH ImageJ revealed that the molar ratio of cysA-C_{10}Acys heterodimers (band 2 in Figure 2.13) to C_{10}Acys homodimers (band 1 in Figure 2.13) is 83.8 ± 7.1% and 85.2 ± 4.0 %, respectively, for solutions at 50 μM and 100 μM, suggesting that the majority of the tetrameric aggregates contain antiparallel leucine zipper strands.

4. Discussion

The low values of G'_{∞}/nkT (less than 13%) under all conditions examined suggest that the elastically effective chain fraction is low in $AC_{10}A$ hydrogels (Figure 2.2-2.4). On a molecular level, the most likely explanation is that $AC_{10}A$ chains tend to form a substantial fraction of looped configurations that do not contribute to network elasticity[1]. The tendency of $AC_{10}A$ chains to form loops is supported by the significant quenching of the fluorescence of an N-terminal tryptophan by a C-terminal coumarin (Figure 2.9). Loops in $AC_{10}A$ hydrogels and the consequent low plateau storage moduli are governed by the structural features of different domains, including the aggregation number of the

associative leucine zipper domain, the relative orientation of leucine zipper strands in each aggregate, and the dimensions of the midblock.

Compared to chemical associative groups that lead to transient networks, leucine zipper domains are unique in that their aggregation numbers are small. Naturally occurring leucine zipper domains oligomerize into dimers, trimers, tetramers or pentamers[37,38]. Higher order aggregation has not been reported, probably due to the narrow hydrophobic face on each strand. Tetrameric association of leucine zipper A was revealed from multi-angle static light scattering of AC_{10}trp solutions (Figure 2.10), in accord with prior findings of Kennedy[26]. This small aggregation number makes elastically effective chain fraction very sensitive to intramolecular association, contributing to the exceptionally low plateau storage moduli of $AC_{10}A$ networks. As shown in Figure 2.14, an aggregate that contains one looped chain only has two arms and simply links two chains into one elastically effective chain. Although three chains are connected to the aggregate, only 1/3 of them can be counted as elastically effective.

The sensitivity of elastically effective chain fraction to loop formation due to the small aggregation number, combined with a tendency to form loops due to compact dimensions of the midblock, leads to low G'_∞/nkT. Quasi-elastic light scattering of a C_{10}trp solution revealed the radius of gyration and the average end-to-end distance of the C_{10} domain to be ca. 24~30 Å and 59~73 Å, respectively. Since the leucine zipper A associates into tetramers, the center-to-center distance between leucine zipper aggregates in a 7% w/v $AC_{10}A$ solution is approximately 100 Å (Figure 2.15). To avoid the energy penalty for stretching the midblock, the chains tend to form loops.

The mean hydrodynamic radius of the C_{10} domain is 20 Å as revealed from quasi-elastic light scattering. The dimension distribution revealed from CONTIN analysis suggests that chains of hydrodynamic radius as small as 13 Å exist (R_g≈16-20 Å and $\sqrt{\langle R^2 \rangle}$≈38-48 Å). Since the length of the leucine zipper helices is ca. 65 Å[25], in order for these chains to form loops, their two zipper domains must adopt antiparallel orientations (N→C/C→N) in tetrameric aggregates so that the midblock is not stretched. However, protein associative domains can discriminate between parallel and antiparallel orientations in aggregates. The hypothesis that the loop fraction is substantial in $AC_{10}A$ networks is only plausible if the A domains can accommodate antiparallel configurations. Therefore, it is particularly significant that antiparallel configurations were evident in both FRET of donor/acceptor labeled A (Figure 2.7-2.8) and the formation of heterodimers of cysA/C_{10}Acys in thiol-disulfide exchange experiments (Figure 2.13).

The importance of midblock chain dimensions for the loop-to-bridge ratio is evident in the effects of concentration, pH and salt on G'_∞. With increasing concentration, if the topology of the network (i.e. the loop-to-bridge ratio) did not change, G'_∞/nkT would be constant. Instead, G'_∞/nkT increases with concentration (Figure 2.2): as the average distance between leucine zipper aggregates decreases, the penalty for stretching the midblock to span aggregates becomes less severe, so the loop-to-bridge ratio decreases, leading to an increase in G'_∞/nkT.

The nonmonotonic effect of pH on G'_∞ at first seems surprising. With increasing pH, leucine zipper association becomes weaker, as indicated by faster strand exchange and network relaxation (discussed in Chapter III). This would intuitively suggest that materials either retain constant rigidity or even become softer as pH increases, because

destabilized leucine zipper association could decrease network connectivity. The increase in modulus as pH increases from 7 to 8 (Figure 2.3) must originate instead from changes in the midblock, a random coil polyelectrolyte. To examine the effect of pH on the midblock, a histidine-tag-free C_{10}trp solution was titrated. The titration result suggests that deprotonation of the glutamic acid residues in the midblock extends into the pH regime between 7.0 and 8.0 (Figure 2.12). Thus, the pH range in which G'_∞ increases coincides with an increase in electrostatic repulsion in the midblock due to the increase in negatively charged glutamic acid residues. In chemically crosslinked polyelectrolyte networks that have fixed topology, storage modulus decreases when electrostatic repulsion among chain segments increases[39,40], because less external energy (stress) is required to stretch the chain to the same extent (strain). The atypical trend exhibited by $AC_{10}A$ networks can only be explained through changes in topology. The increased electrostatic repulsion results in an expansion in the midblock, which reduces the loop-to-bridge ratio and consequently increases G'_∞/nkT (Figure 2.3 (b)).

The increase in modulus with increased electrostatic repulsion in the midblock in response to pH is in accord with the increase in modulus with reduced salt concentration (Figure 2.4). The buffer of lower ionic strength has less screening effect on electrostatic repulsion, yielding more expanded midblock dimensions, which reduces the loop-to-bridge ratio and consequently increases G'_∞/nkT.

Understanding structural features of the building blocks of $AC_{10}A$ and their effects on material properties provide molecular design guidelines to increase material rigidity by tuning the structure of the midblock (as shown below) and the endblocks (as discussed in Chapter IV). Based on the importance of network topology, we anticipated

that midblock with a longer contour length or a higher charge density would favor bridges over loops and lead to networks exhibiting greater plateau storage moduli than $AC_{10}A$ hydrogels. Two new triblock proteins, $AC_{26}A$ and $A[AGPEG]_{18}A$, were synthesized. Indeed, both of them assembled into hydrogels that had G'_∞ roughly twice that of $AC_{10}A$ hydrogels (Figure 2.5-2.6). Although increasing the chain length between crosslinking points generally decreases network elasticity of rubber and gel materials[29], the plateau storage moduli of $AC_{10}A$ and $AC_{26}A$ hydrogels show an opposite trend. This is because plateau storage moduli of these hydrogels are determined by two competing factors: the total chain number density and the elastically effective chain fraction. When the midblock C_{10} is replaced by C_{26}, the increase in the fraction of elastically effective chains overcomes the decrease in the number density of chains and leads to a greater plateau storage modulus.

5. Conclusions

Network topology plays a dominant role in determining storage moduli of $AC_{10}A$ hydrogels. $AC_{10}A$ chains have a strong tendency to form loops due to the compact random coil midblock (mean R_H~2.0 Å) and the ability of the leucine zipper A domains to adopt antiparallel orientation in aggregates. Furthermore, loop formation has unusually pronounced effects on G'_∞ because of the small aggregation number (tetrameric association). Understanding the importance of the loop-to-bridge ratio in the network provides a unified explanation of the intriguing effects of concentration, pH and ionic strength on G'_∞. Physical insights into the structure-property relationships led to successful design strategies to control material properties by tuning different building

blocks. In particular, contrary to the behavior of conventional gels, the plateau storage modulus increased when the midblock C_{10} was replaced by new polypeptides with either a greater contour length or a higher charge density.

6. References

(1) Annable, T.; Buscall, R.; Ettelaie, R.; Whittlestone, D. *Journal of Rheology* **1993**, *37*, 695-726.

(2) Kim, S. W.; Bae, Y. H.; Okano, T. *Pharmaceutical Research* **1992**, *9*, 283-290.

(3) Kim, S. W. *Pharmacy International* **1983**, *4*, 182-182.

(4) Jen, A. C.; Wake, M. C.; Mikos, A. G. *Biotechnology and Bioengineering* **1996**, *50*, 357-364.

(5) Lee, K. Y.; Mooney, D. J. *Chemical Reviews* **2001**, *101*, 1869-1879.

(6) Lauffenburger, D. A.; Griffith, L. G. *Proceedings of the National Academy of Sciences of the United States of America* **2001**, *98*, 4282-4284.

(7) Hench, L. L.; Polak, J. M. *Science* **2002**, *295*, 1014-+.

(8) Drury, J. L.; Mooney, D. J. *Biomaterials* **2003**, *24*, 4337-4351.

(9) Petka, W. A.; Harden, J. L.; McGrath, K. P.; Wirtz, D.; Tirrell, D. A. *Science* **1998**, *281*, 389-392.

(10) Surks, H. K.; Richards, C. T.; Mendelsohn, M. E. *Journal of Biological Chemistry* **2003**, *278*, 51484-51493.

(11) O'Shea, E. K.; Rutkowski, R.; Stafford, W. F.; Kim, P. S. *Science* **1989**, *245*, 646-648.

(12) Wong, J. Y.; Velasco, A.; Rajagopalan, P.; Pham, Q. *Langmuir* **2003**, *19*, 1908-1913.

(13) Lo, C. M.; Wang, H. B.; Dembo, M.; Wang, Y. L. *Biophysical Journal* **2000**, *79*, 144-152.

(14) Geiger, B.; Bershadsky, A. *Current Opinion in Cell Biology* **2001**, *13*, 584-592.

(15) Engler, A.; Bacakova, L.; Newman, C.; Hategan, A.; Griffin, M.; Dischery, D. *Biophysical Journal* **2004**, *86*, 617-628.

(16) Petka, W. A.; Ph.D. Dissertation; University of Massachusetts Amherst: Amherst, MA 1997.

(17) Tang, Y.; Ph.D. Dissertation; California Institute of Technology: Pasadena, 2002.

(18) Liou, Y. M.; Jiang, M. J.; Wu, M. C. *Journal of Biochemistry* **2002**, *132*, 317-325.

(19) Huglin, M. B. *Light scattering from polymer solutions*; Academic Press: London, New York, 1972.

(20) Saghatelian, A.; Yokobayashi, Y.; Soltani, K.; Ghadiri, M. R. *Nature* **2001**, *409*, 797-801.

(21) Ferry, J. D. *Viscoelastic properties of polymers*; Wiley: New York, 1980.

(22) B. Wieb van der Meer, G. C. I., S.-Y. Simon Chen. *Resonance energy transfer : theory and data*; VCH: New York, 1994.

(23) Garcia, R. A.; Forde, C. E.; Godwin, H. A. *Proceedings of the National Academy of Sciences of the United States of America* **2000**, *97*, 5883-5888.

(24) Trakselis, M. A.; Roccasecca, R. M.; Yang, J. S.; Valentine, A. M.; Benkovic, S. J. *Journal of Biological Chemistry* **2003**, *278*, 49839-49849.

(25) Hodges, R. S. *Biochemistry and Cell Biology-Biochimie Et Biologie Cellulaire* **1996**, *74*, 133-154.

(26) Kennedy, S. B.; Ph.D. Dissertation; University of Massachusetts Amherst: Amherst, MA 2001.

(27) Oono, Y.; Kohmoto, M. *Journal of Chemical Physics* **1983**, *78*, 520-528.

(28) Doi, M. *Introduction to polymer physics*: Oxford : Clarendon Press ; New York : Oxford University Press, 1996.

(29) Flory, P. J. *Principles of polymer chemistry*; Cornell University Press: Ithaca, N.Y., 1953.

(30) Jannink, J. d. C. a. G. *Polymers in solution : their modelling and structure*: Oxford : Clarendon Press ; New York : Oxford University Press, 1990.

(31) Kosmas, M. K. *Journal of Physics a-Mathematical and General* **1981**, *14*, 2779-2788.

(32) Mattice, W. L.; Mandelke.L. *Biochemistry* **1971**, *10*, 1934-&.

(33) Brant, D. A.; Flory, P. J. *Journal of the American Chemical Society* **1965**, *87*, 2791-&.

(34) Tanford, C.; Kawahara, K.; Lapanje, S. *Journal of Biological Chemistry* **1966**, *241*, 1921-&.

(35) Brant, D. A.; Flory, P. J. *Journal of the American Chemical Society* **1965**, *87*, 2788-&.

(36) Urry, D. W. *Journal of Physical Chemistry B* **1997**, *101*, 11007-11028.

(37) Harbury, P. B.; Zhang, T.; Kim, P. S.; Alber, T. *Science* **1993**, *262*, 1401-1407.

(38) Malashkevich, V. N.; Kammerer, R. A.; Efimov, V. P.; Schulthess, T.; Engel, J. *Science* **1996**, *274*, 761-765.

(39) Rubinstein, M.; Colby, R. H.; Dobrynin, A. V.; Joanny, J. F. *Macromolecules* **1996**, *29*, 398-406.

(40) Dobrynin, A. V.; Colby, R. H.; Rubinstein, M. *Macromolecules* **1995**, *28*, 1859-1871.

Scheme 2.1. Amino acid sequences of proteins discussed in chapter II

AC_{10}Atrp (or AC_{10}A):
MRGSHHHHHHGSDDDDKASGDLENEVAQLEREVRSLEDEAAELEQKVSRLKNEIEDLKAEIGDHVAPRDTSYRDPMG
[AGAGAGPEG]$_{10}$ARMPTSGDLENEVAQLEREVRSLEDEAAELEQKVSRLKNEIEDLKAEIGDHVAPRDTSW

AC_{10}Acys (or W-AC_{10}A):
MRGSHHHHHHGSDDDDKWASGDLENEVAQLEREVRSLEDEAAELEQKVSRLKNEIEDLKAEIGDHVAPRDTSYRDP
MG[AGAGAGPEG]$_{10}$ARMPTSGDLENEVAQLEREVRSLEDEAAELEQKVSRLKNEIEDLKAEIGDHVAPRDTSMGGC

AC_{10}A-no-trp:
MRGSHHHHHHGSMASGDLENEVAQLEREVRSLEDEAAELEQKVSRLKNEIEDLKAEIGDLNNTSYRDPMG[AGAGAG
PEG]$_{10}$ARMPTSGDLENEVAQLEREVRSLEDEAAELEQKVSRLKNEIEDLKAEIGDLNNTSGIRRPAAKLN

Acys (or W-A):
MRGSHHHHHHGSDDDDKWASGDLENEVAQLEREVRSLEDEAAELEQKVSRLKNEIEDLKAEIGDHVAPRDTSMGGC

Atrp:
MRGSHHHHHHGSDDDDKASYRDGDLENEVAQLEREVRSLEDEAAELEQKVSRLKNEIEDLKAEIGDPRMPTSW

cysA:
MCGSHHHHHHGSDDDDKASYRDGDLENEVAQLEREVRSLEDEAAELEQKVSRLKNEIEDLKAEIGDPRMPTSW

C_{10}trp:
MRGSHHHHHHGSDDDDKASYRDPMG[AGAGAGPEG]$_{10}$ ARMPTSW

C_{10}Acys:
MRGSHHHHHHGSDDDDKWASYRDPMG[AGAGAGPEG]$_{10}$ARMPTSGDLENEVAQLEREVRSLEDEAAELEQKVSRLK
NEIEDLKAEIGDHVAPRDTSMGGC

AC_{10}trp:
MRGSHHHHHHGSDDDDKASGDLENEVAQLEREVRSLEDEAAELEQKVSRLKNEIEDLKAEIGDHVAPRDTSYRDPMG
[AGAGAGPEG]$_{10}$ ARMPTSW

AC_{26}Atrp:
MRGSHHHHHHGSDDDDKASGDLENEVAQLEREVRSLEDEAAELEQKVSRLKNEIEDLKAEIGDHVAPRDTSYRDPMG
[AGAGAGPEG]$_{26}$ARMPTSGDLENEVAQLEREVRSLEDEAAELEQKVSRLKNEIEDLKAEIGDHVAPRDTSW

A[AGPEG]$_{18}$Atrp:
MRGSHHHHHHGSDDDDKASGDLENEVAQLEREVRSLEDEAAELEQKVSRLKNEIEDLKAEIGDHVAPRDTSYRDPMG
[AGPEG]$_{18}$ARMPTSGDLENEVAQLEREVRSLEDEAAELEQKVSRLKNEIEDLKAEIGDHVAPRDTSW

Abbreviation for domains:
A: S(D)GDLENEVAQLEREVRSLEDEAAELEQKVSRLKNEIEDLKAE
$C_{10\ (26)}$: [AGAGAGPEG]$_{10\ (26)}$
His-tag: HHHHHH

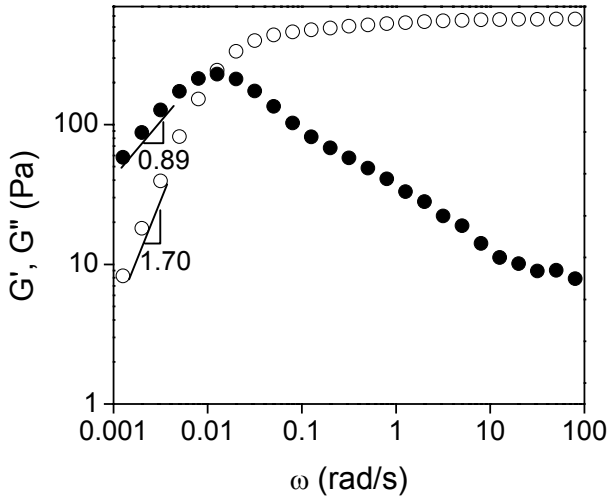

Figure 2.1. Dynamic moduli of an $AC_{10}A$ hydrogel. (7% w/v, pH 8.0, 100 mM phosphate buffer, 22 °C) ○ G′; ● G″.

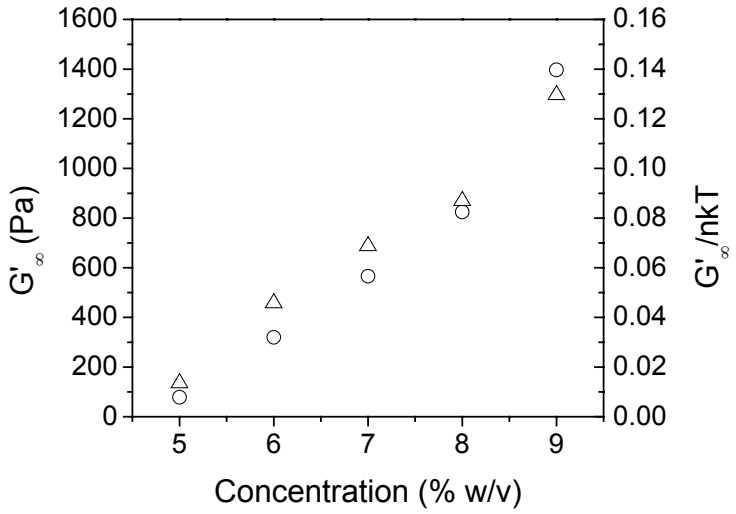

Figure 2.2. Concentration dependence of plateau storage moduli of $AC_{10}A$ hydrogels (pH 8.0, 100 mM phosphate buffer, 22 °C) ○ G′; △ G′/nkT.

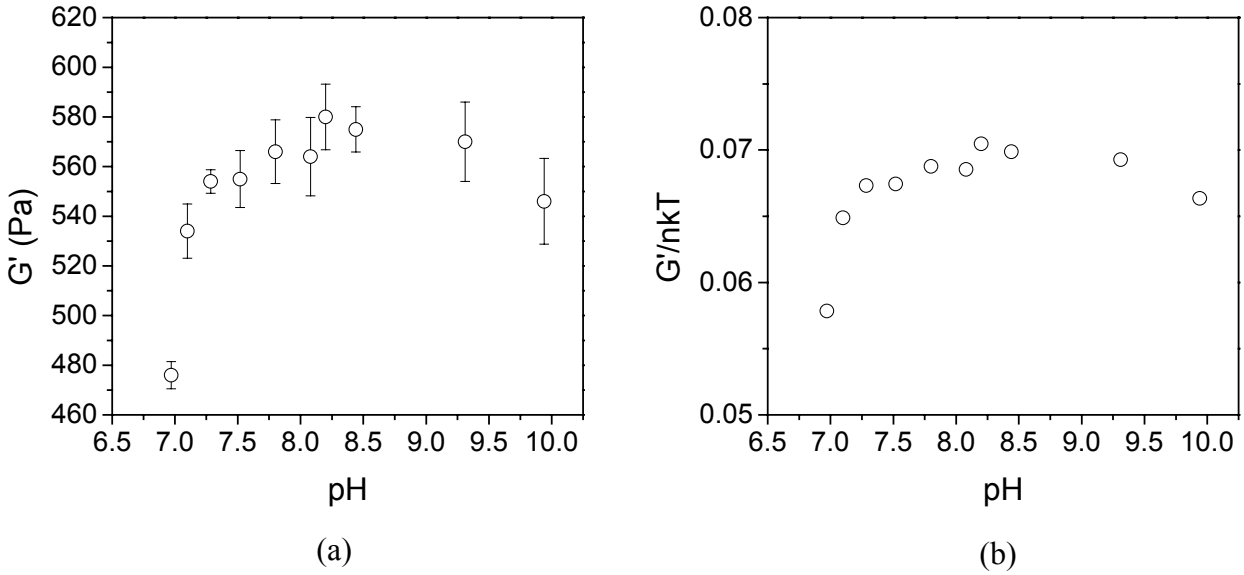

(a) (b)

Figure 2.3. Effect of pH on plateau storage moduli of $AC_{10}A$ hydrogels. (7% w/v, 100 mM phosphate buffer, 22 °C) (a) G'_{∞}; (b) G'_{∞} /nkT.

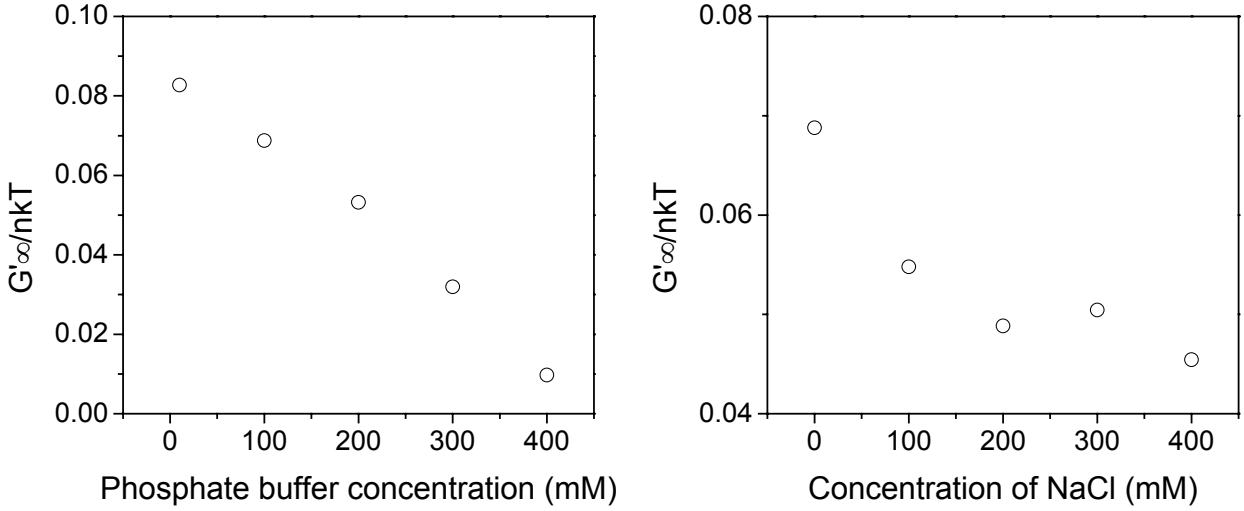

(a) (b)

Figure 2.4. Effects of buffer and salt concentrations on plateau storage moduli of $AC_{10}A$ hydrogels (7% w/v, pH 8.0, 22 °C) (a) phosphate buffer; (b) different NaCl concentrations in addition to 100 mM phosphate buffer.

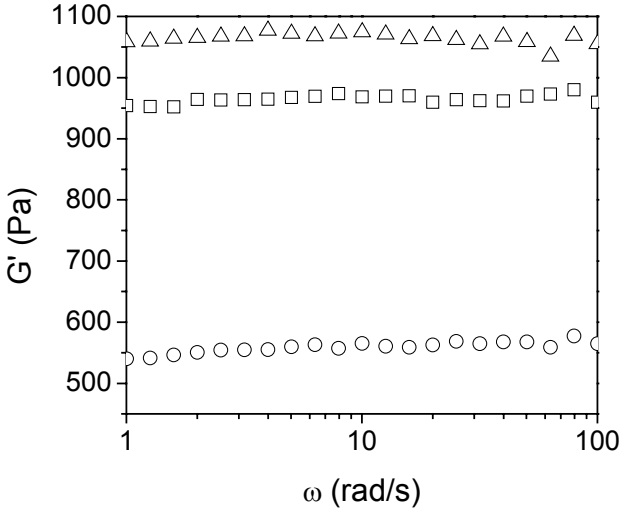

Figure 2.5. Storage moduli of $AC_{10}A$ (○); $AC_{26}A$ (□); and $A[AGPEG]_{18}A$ hydrogels (△). (7% w/v, pH 8.0, 100 mM phosphate buffer, 22 °C)

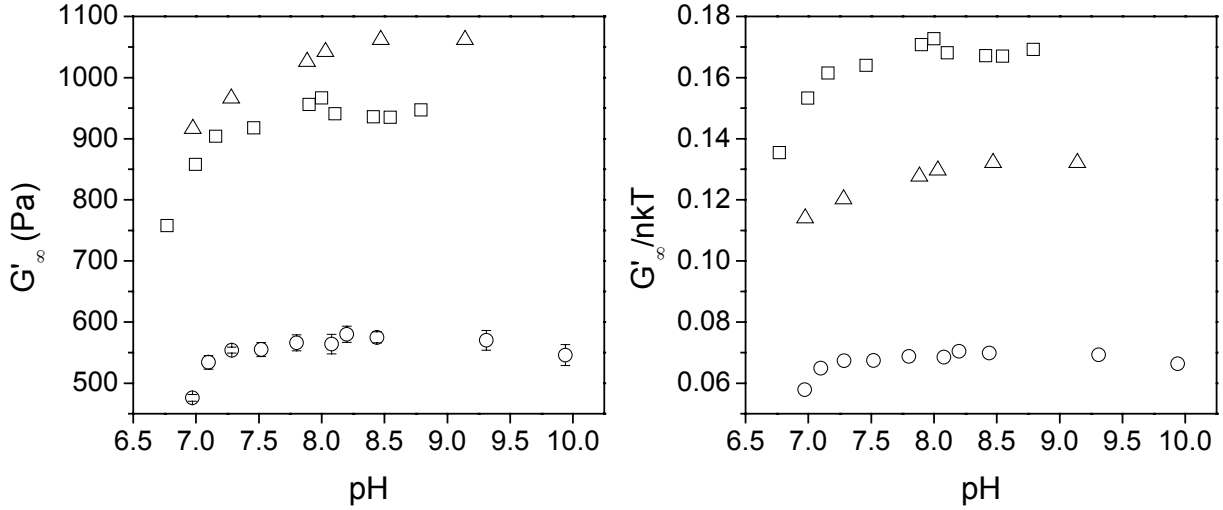

Figure 2.6. Plateau storage moduli of $AC_{10}A$ (○); $AC_{26}A$ (□); and $A[AGPEG]_{18}A$ (△) hydrogels at different pH. (7% w/v, 100mM phosphate buffer, 22 °C)

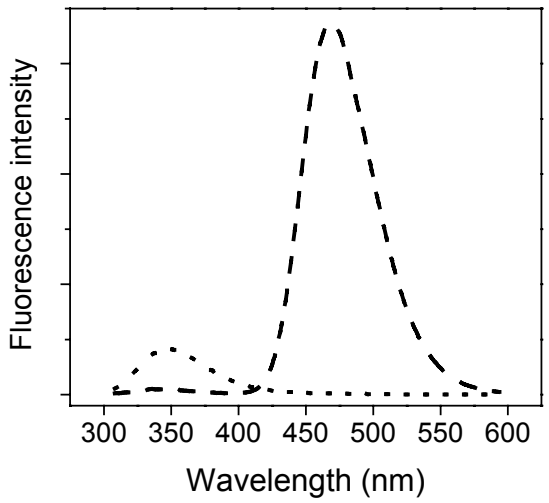

Figure 2.7. Fluorescence emission from solutions of leucine zipper A containing a N-terminal tryptophan in the absence (·····) and presence (**--**) of C-terminal coumarin. (100 μM protein, 100 mM phosphate buffer, pH 7.6, 22 °C, the baseline was subtracted)

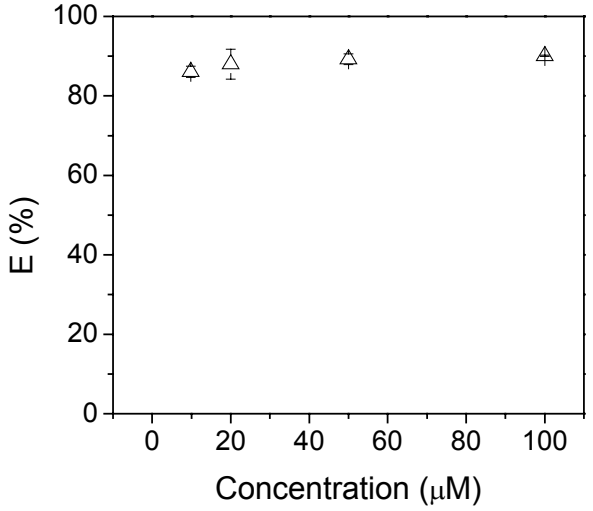

Figure 2.8. Fluorescence energy transfer efficiency in W-A-CPM solutions at various concentrations. (100 mM phosphate buffer, pH 7.6, 22 °C)

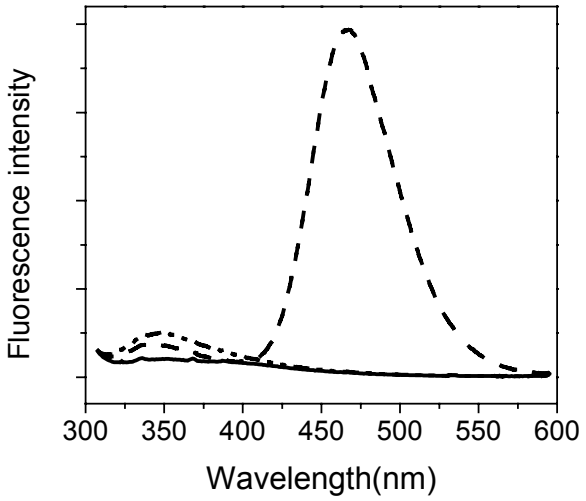

Figure 2.9. The fluorescence of the tryptophan at the N-terminus of $AC_{10}A$ is quenched by the C-terminal coumarin in 1.05% w/v $AC_{10}A$-no-trp solutions. ━ $AC_{10}A$-no-trp; ··· $AC_{10}A$-no-trp + W-$AC_{10}A$; ╍ $AC_{10}A$-no-trp + W-$AC_{10}A$-CPM. (in each solution the molar ratio of the tryptophan-containing $AC_{10}A$ to $AC_{10}A$-no-trp is 1:25, 100 mM phosphate buffer, pH 7.6, 22 °C)

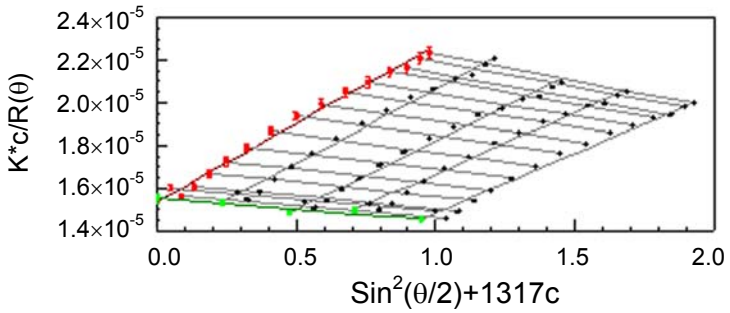

Figure 2.10. Zimm plot of multi-angle light scattering signals from AC_{10}trp solutions. Concentrations of the solutions subjected to measurements are 11 μM, 22 μM, 33 μM and 44 μM, respectively. (100 mM phosphate buffer, pH 7.6, 22 °C.) The molar mass of the dominant species in the solutions is 64740 Da, suggesting tetrameric association. (The molar mass of monomer AC_{10}trp is 16334 Da.)

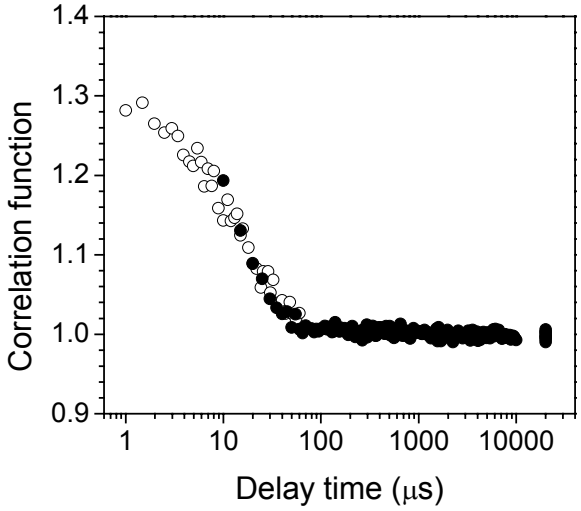

Figure 2.11. Time correlation function of a C_{10}trp solution (pH 10.0, 140 μM) revealed from quasi-elastic light scattering measurements. ● from Brookhaven BI-9000AT digital autocorrelator (Sample were filtered through 0.02 μM filters); ○ from Wyatt WyattQELS digital autocorrelator (Samples were not filtered through 0.02 μM filters. The data points deflect at the same delay time (ca. 60 μs) as those from BI-9000AT autocorrelator, but exhibit a small tail before reach a flat baseline. The signals in the tail (from impurity particles) were ignored.). Analysis of the correlation function on the basis of the CONTIN algorithm suggests an R_H of 2.0 ± 0.03 nm.

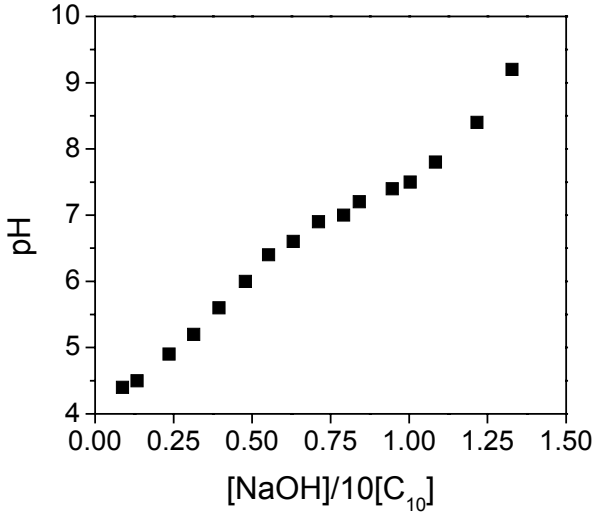

Figure 2.12. Titration curve for the polypeptide $G[(AG)_3PEG]_{10}ARM$ (C_{10}). (662.5 μM in water)

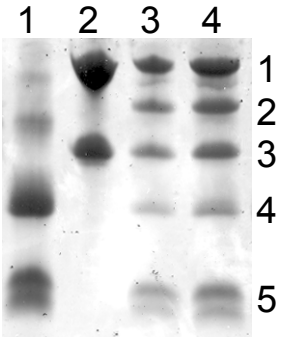

Figure 2.13. Electrophoresis of mixtures of cysA and C_{10}Acys revealed antiparallel leucine zipper strands in aggregates. Lane: 1. cysA (200 μM); 2. C_{10}Acys (200 μM); 3. mixture of cysA (50 μM) and C_{10}Acys (50 μM) with addition of redox buffer; 4. mixture of cysA (100 μM) and C_{10}Acys (100 μM) with addition of redox buffer. Band: 1. dimer of C_{10}Acys linked by a disulfide bond; 2. cysA and C_{10}Acys heterodimer linked by a disulfide bond; 3. monomer C_{10}Acys; 4. dimer of cysA linked by a disulfide bond; 5. monomer cysA. The molar ratio of the protein in band 2 to that in band 1 is 83.8 ± 7.1% and 85.2 ± 4.0 %, respectively, for lane 3 (50 μM) and lane 4 (100 μM) based on an analysis using NIH ImageJ (assuming identical staining for different domains).

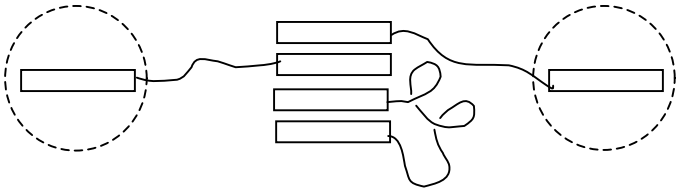

Figure 2.14. The small aggregation number makes the elastically effective chain fraction very sensitive to intramolecular association. Although three chains are connected to the aggregate, only 1/3 of them can be counted as elastically effective.

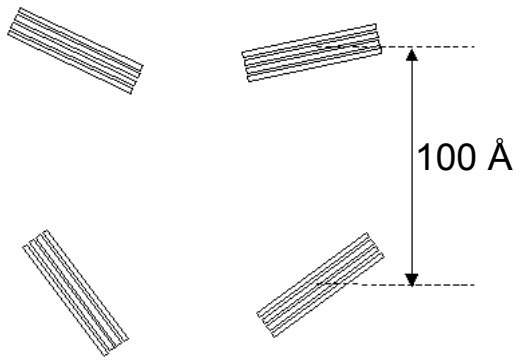

Figure 2.15. The center-to-center distance between leucine zipper aggregates in a 7% w/v $AC_{10}A$ solution is approximately 100 Å based on an assumption of cubic structure in the packing of aggregates.